JOURNAL OF PROPULSION AND POWER
Vol. 23, No. 3, May–June 2007

Experimental Investigations of the Performance and Unsteady Behavior of a Supersonic Intake

Christian Hirschen,* Dirk Herrmann,* and Ali Gülhan*
German Aerospace Center, 51170 Köln, Germany

DOI: 10.2514/1.25103

The performance and the unsteady behavior of a ramjet intake model have been investigated. The investigation was carried out in the supersonic flow range of the trisonic wind tunnel of the German Aerospace Center. These experiments were conducted to understand the complex flow phenomena of the ramjet intake and the effects on the performance. The experiments were carried out on a ramjet designed for a shock on lip Mach number of $M = 2.5$. To study the effect of the shock boundary layer interaction on the performance, four different bleed configurations of the boundary layer were used. The effect on performance and the unsteady behavior of each geometry variation were investigated and compared to find the optimum intake design. Pressure and temperature measurements were taken of the performance and the unsteady behavior using mass flow determination and shown with high-speed schlieren photographs.

Nomenclature

A	=	area
f	=	frequency
H	=	throat height
l_{ch}	=	characteristic length
$\dot{m}$	=	mass flow
p	=	pressure
R	=	gas constant of air
T	=	temperature
t	=	time
v	=	flow velocity
x, y	=	Cartesian coordinates
α	=	angle of attack
κ	=	heat capacity ratio
ρ	=	density

Subscripts

0	=	plane in front of the intake
3	=	cross section with pressure measurements
4	=	critical cross section of the throttle
min	=	minimum
st	=	static
t	=	total

I. Introduction

TWO of the main current research goals in the field of aeronautics and astronautics are to reduce the high cost of space missions and to increase the reliability of airplanes and space vehicles. The propulsion units of both airplanes and space vehicles have highly complex and costly components. For supersonic flights, ramjet technology is one of the most investigated [1] airbreathing engine concepts. Ramjet engines can be used as an effective alternative to solid and fluid-propellant rockets [2]. The advantages of the ramjet engine are weight reduction because the ramjet uses oxygen from the atmosphere, and an increase of the payload–mass ratio [3].

Investigation is still required to find the solution for some aspects of the design of the ramjet. Examples are the performance of the intake influenced by the shock boundary layer interactions [4,5], spillage effects during off-design operation, and the unsteady behavior (buzzing) of the ramjet intakes in certain flight configurations. These typical flow phenomena have a great effect on the performance characteristics of the intake, that is, the pressure recovery and the mass flow rate [6–8]. Several experimental and numerical studies have shown that bleeding can control the boundary layer growth and boundary layer separation, caused by shock impingement [9–12]. Research into the level of buzzing that the intake of the ramjet must withstand is also of great importance. This strong buzzing can lead to a destruction of the intake and must be avoided [13].

This paper makes an in-depth investigation of the intake flow and flow phenomena for the shock systems, boundary layer separation, and buzzing. Also the effects of different bleed modes on the boundary layer growth, boundary layer separation, and buzzing frequencies are investigated and compared for the ramjet intake used for the experiment.

The present work also investigates the buzzing frequencies due to different intake geometries by using pressure measurements and the high-speed schlieren photographic techniques. To gain a better understanding of the buzzing phenomenon, experiments with different geometry configurations for one intake were made in the blowdown wind tunnel Transsonische Messstrecke Köln (TMK) of the German Aerospace Center in Cologne. The buzzing frequencies of the different configurations were studied with steady and unsteady pressure measurements as well as high-speed schlieren photography techniques. The results show that the buzzing frequency depends on the geometry of the intakes. The frequency is greatly influenced by the bleed gap; the difference in the buzzing frequency with a bleed gap and without a bleed gap is significant.

In addition to buzzing, further unsteady phenomena in the intake could be observed with the high-speed schlieren technique. This phenomena is caused by the separation of the boundary layer inside the slightly divergent diffuser. The unsteadiness leads to pressure losses and therefore a reduction of the performance of the intake.

II. Test Model and Measurement Technique

The experiments use a ramjet intake as shown in Fig. 1. The shock on lip Mach number for this intake is $M = 2.5$. The elements of the ramjet intake are shown in the front and side views in Fig. 1. Inside the intake there is a ramp, bleed duct, and subsonic diffuser. The ramp and subsonic diffuser are adjustable. The ramp is set to a fixed position and the bleed duct is located downstream from the ramp. The

Received 15 May 2006; accepted for publication 8 November 2006. Copyright © 2007 by Christian Hirschen. Published by the American Institute of Aeronautics and Astronautics, Inc., with permission. Copies of this paper may be made for personal or internal use, on condition that the copier pay the $10.00 per-copy fee to the Copyright Clearance Center, Inc., 222 Rosewood Drive, Danvers, MA 01923; include the code 0748-4658/07 $10.00 in correspondence with the CCC.

*Wind Tunnel Department of the Institute of Aerodynamics and Flow Technology, Linder Höhe.

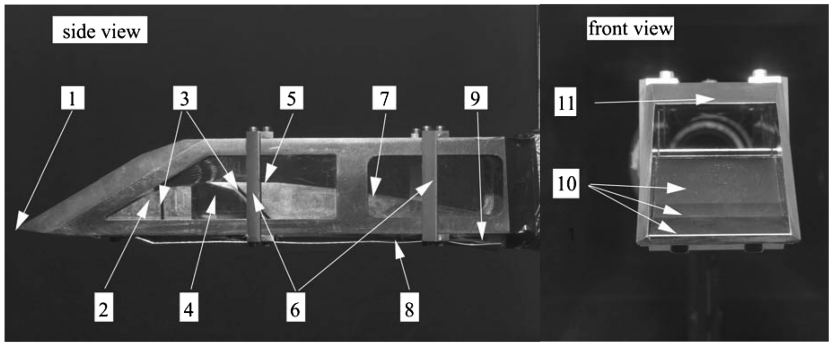

Fig. 1 Side and front view of the model.

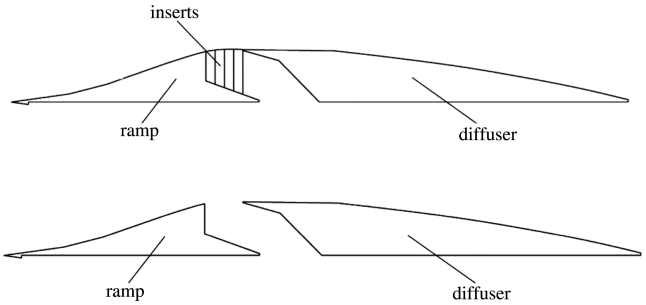

Fig. 2 Configurations I4 (0|0) (top), I0 (0|0) (bottom).

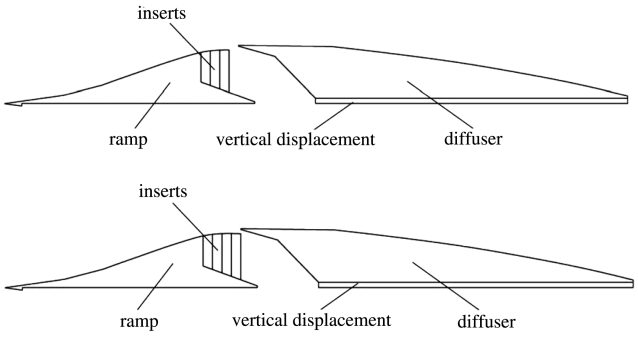

Fig. 3 Configurations I3 (5.4|3) (top), I4 (5.4|3) (bottom).

size of the bleed duct can be changed by four removable bleed inserts that are attached to the ramp (Fig. 2). The subsonic diffuser can be installed at three different horizontal positions that also give a variation to the size and position of the bleed gap. The vertical position of the subsonic diffuser can be adjusted with washers (Fig. 3). From these possible variations of the intake geometry, four configurations were tested. These variations are listed and explained in Table 1.

The isolator separates the diffuser from the throat section. The isolator has a slightly divergent angle of -1 deg that minimizes the effect of the growing boundary layer. This angle allows a constant effective-flow cross-sectional area and a flow stream with a constant Mach number of $\mathrm{d}M/\mathrm{d}x = 0$. This prevents an unstable shock position depending on the throttle position. The throttle is used to adjust the pressure level at the diffuser exit of these experiments without the combustion to the operational pressure level of an operational ramjet.

To measure the buzzing frequencies for the different intake configurations, Kulite pressure transducers were installed inside the diffuser. These transducers enabled distribution measurements of the unstable pressures to be taken. Kulite pressure transducers with a range of 50 psi were used for these experiments. The level of accuracy obtained by the Kulite pressure transducers is $\pm 0.1\%$. To obtain high-resolution data, transducers with a natural response frequency of 500 kHz were installed close to the flow surface of the model. According to Wuest [14] there is a direct linear relationship between the response time and the length of the pressure measurement tube, therefore the pressure transducers had to be placed as close to the flow surface of the model as possible.

The performance of different intake configurations is determined by measurements of the pressure recovery and air mass flow rate. At the diffuser end, a throttle is used to regulate the intake exit pressure. The pressure recovery $p_{t,3}/p_{t,0}$ and the mass flow rate $\dot{m}_3/\dot{m}_0$ vary by the throttle position. This variation is shown by the performance chart; refer to Fig. 4. The y axis in this chart shows the pressure recovery $p_{t,3}/p_{t,0}$; the x axis shows the mass flow rate $\dot{m}_3/\dot{m}_0$. The chart shows the comparison of the performance between the four different configurations. To calculate the pressure recovery and the mass flow rate, it was necessary to measure the static pressure directly before the critical cross section at the throttle. Using the measurement of the static pressure $p_{\mathrm{st},3}$, the cross-sectional area A_3, and the $M_4 = 1$ (sonic) condition in the critical cross section, the pressure recovery $p_{t,3}/p_{t,0}$ and the mass flow rate $\dot{m}_3/\dot{m}_0$ can be calculated with Eqs. (1–3).

$$\dot{m}_0 = \frac{p_{\mathrm{st},0}}{\sqrt{RT_t}} A_0 M_0 \sqrt{RT_t \kappa} \tag{1}$$

$$\dot{m}_3 = \frac{p_{\mathrm{st},3}}{\sqrt{RT_t}} A_3 M_3 \sqrt{\kappa} \sqrt{1 + \frac{\kappa - 1}{2} M_3^2} \tag{2}$$

$$p_{t,3} = p_{\mathrm{st},3} \left(1 + \frac{\kappa - 1}{2} M_3^2 \right) \tag{3}$$

The mass flow $\dot{m}_3$ is calculated from the measured value of the static pressure $p_{\mathrm{st},3}$, the cross-sectional area A_3, and the total temperature T_t. Nevertheless, the Mach number M_3 has first to be computed iteratively by applying the continuity equation Eq. (4)

Table 1 The four bleed configurations

Name	Bleed inserts	Diffuser		Size of bleed gap	
		Horizontal displacement, mm	Vertical displacement, mm	x direction, mm	y direction, mm
I4 (0|0)	4	0	0	0	0
I0 (0|0)	0	0	0	21.6	0
I3 (5.4|3)	3	5.4	3	10.8	3
I4 (5.4|3)	4	5.4	3	5.4	3

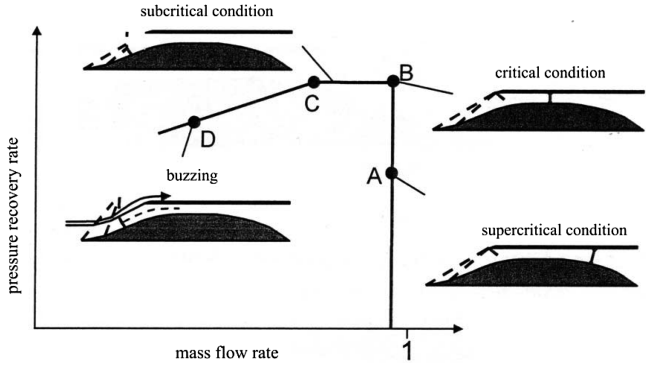

Fig. 4 Intake performance curve in different operation modes [19].

between the cross-sectional area A_3 where the static pressure $p_{st,3}$ is measured and the critical cross section A_4. The index number "0" refers to the plane in front of the intake where the free stream conditions are valid. The index number "3" refers to the plane in the throttle where the static pressure $p_{st,3}$ is measured.

$$\dot{m}_3 = \dot{m}_4 \tag{4}$$

The measurement inaccuracies of the aforementioned performance data are presented as follows: $\Delta p_{st,3}/p_{st,3} = 0.02\%$, $\Delta A_3/A_3 = 0.02\%$, $\Delta(p_{t,3}/p_{t,0})/(p_{t,3}/p_{t,0}) = 0.03\%$, and $\Delta(\dot{m}_3/\dot{m}_0)/(\dot{m}_3/\dot{m}_0) = 1.16\%$. Although the pressure measurements are quite accurate, the determination of the mass flow rate requires a calibration procedure using a standard calibration unit as reference. The preceding inaccuracies are very close to the values of the mass flow calibration unit.

The schlieren photographs [15,16] were taken, using a single lens reflex (SLR) camera with a high spatial resolution and a high-speed capability. The camera is able to take sharp images with high frequency of frames per second (fps). The high-speed camera used was a Photron Fastcam Ultima APX-RS. This camera has a resolution of 1024×1024 pixels at a frame rate of 3000 fps. The maximum frame rate is 250,000 fps at a resolution of 128×16 pixel. The SLR camera has a capability of a resolution of 6×10^6 pixels, but with a small frame rate.

III. Experimental Facility and Flow Conditions

The experiments were conducted in the trisonic (sub-, trans-, and supersonic) wind tunnel TMK [17] of the German Aerospace Center in Cologne. This wind tunnel is a blowdown wind tunnel and is able to provide Mach numbers between 0.5 and 5.7. The cross-sectional area of the wind tunnel is 0.6×0.6 m. The unit Reynolds number (characteristic length $l_{ch} = 1$ m) can be varied between a minimum value of $Re_{1m} = 7 \times 10^6$ and a maximum value of $Re_{1m} = 70 \times 10^6$. The test duration is up to 60 s, depending on the flow conditions. Behind the adjustable diffuser is the subsonic diffuser that ducts the air through a deflection elbow into the 18 m high silencer tower with an integrated ejector. The ejector allows a variation of the Reynolds number by a factor of up to 7.

The main freestream flow parameters used for this study are $M = 2.5$, $T_t = 288$ K, and $p_t = 3.6 \times 10^5$ Pa. The error of measurement of the freestream flow parameters are as follows: $\Delta M/M = 0.50\%$, $\Delta T_t/T_t = 0.75\%$, and $\Delta p_t/p_t = 0.02\%$.

IV. Performance Comparison of Different Configurations

The different conditions of an intake operation are shown in Fig. 2. These conditions are called supercritical, critical, subcritical and buzzing. This description is valid for intakes without bleeding. The picture also shows the positions of the normal shock. During an adjustment to the throttle position to increase the combustion chamber pressure, the pressure recovery increases and the mass flow rate remains constant. This is as a direct result of the movement of the normal shock aft to an area upstream and the decrease of the shock Mach numbers. Smaller Mach numbers cause weaker shocks, therefore less pressure losses. Even for the example of a geometry without the bleed, the mass flow rate $\dot{m}_3/\dot{m}_0$ does not have to equal 1, as spillage at the cowl lip causes some mass flow losses.

The supercritical section ends in the critical point, where the shock is located in the critical throat cross section of the intake, that is, H_{min}. From H_{min}, the intake reaches the subcritical condition when the chamber pressure increases. In this condition the normal shock is upstream of the critical throat cross section but still inside the intake. The decrease of the mass flow rate is related to the stronger spillage caused by the shock induced separation on the intake ramp. A further increase of the combustion chamber pressure leads to the buzzing state, which must be critically avoided during real operation. Otherwise the heavy structural loads can lead to severe damage to the intake. During the buzzing condition the normal shock enters and leaves the intake with a certain frequency, the buzzing frequency. In this condition, the intake alternates between the started and unstarted state.

The following figures show the performance charts of the four different intake geometries defined in Figs. 2 and 3. Schlieren photographs are used to explain the flow phenomena and the results. As stated earlier, the differences between the four configurations are the bleed presence (with and without bleeding), the position of the bleed gap, and the size of the bleed gap. The different geometries have a significant effect on the flow properties inside the intakes.

The first configuration has no bleed gap. From Fig. 5, the maximum mass flow rate is $\dot{m}_3/\dot{m}_0 = 0.96$. At the throttle position with $A_4/A_0 = 0.62$, the pressure recovery is $p_{t,3}/p_{t,0} = 0.6$. When the pressure recovery reaches its maximum the throttle position reads $A_4/A_0 = 0.53$. The maximum pressure recovery reaches $p_{t,3}/p_{t,0} = 0.67$ while the mass flow rate decreases to $\dot{m}_3/\dot{m}_0 = 0.92$. The vertical lines in the subcritical region of the graph are an indication of the start of the buzzing of the intake. These lines show the amplitudes of the buzzing oscillation, represented by the rms value normalized by the total pressure $p_{t,0}$. During the operational mode of the intake this condition must be avoided due to structural loads. In Fig. 6, it is noticeable that there is no shock system inside the intake, which indicates that the flow in the intake did not start. The reason for this is the early separation of the flow on the ramp. This also causes an earlier start of the buzzing as well as higher buzzing frequencies and a poorer performance of the intake. The black stripes found at the right sides of the schlieren images are due to scratches on the schlieren windows of the intake model.

In the second configuration, a bleed gap is made by removing the four inserts. This configuration delays the onset of the buzzing, reduces the buzzing frequency, and improves the performance of the intake. The effects of this configuration I0 (0|0) on the performance chart can be seen in Fig. 7. There are noticeable differences between those two configurations. As a result of the bleed gap, the maximum mass flow rate is decreased to $\dot{m}_3/\dot{m}_0 = 0.93$, whereas the maximum pressure recovery is increased by 0.13 to $p_{t,3}/p_{t,0} = 0.80$. At this point, the throttle position reads $A_4/A_0 = 0.41$. This value is higher compared to the first configuration and indicates that the buzzing of

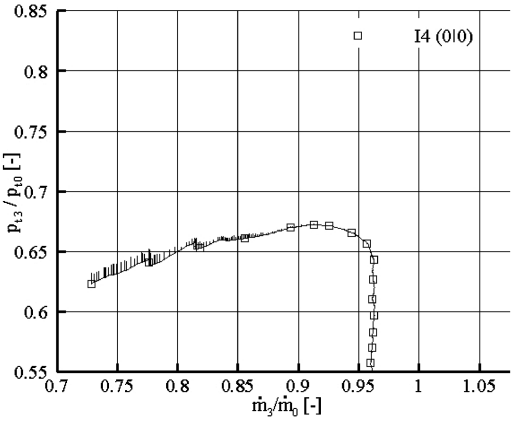

Fig. 5 Performance curve of the configuration I4 (0|0).

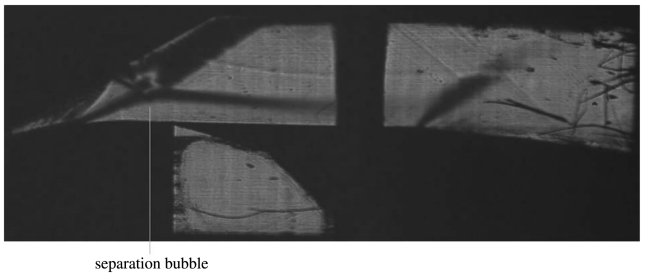

Fig. 6 Flow topology of the configuration I4 (0|0) in nominal operation range (SLR camera).

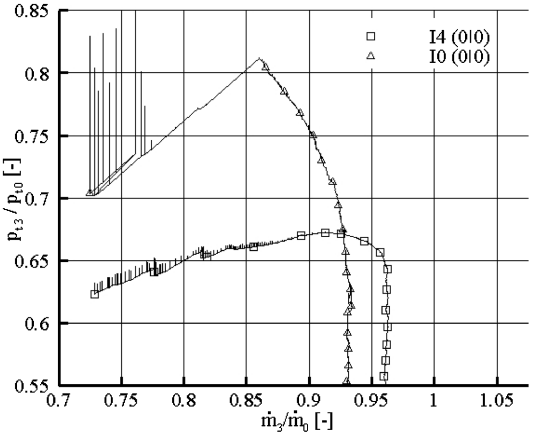

Fig. 7 Performance curves of the configurations I4 (0|0) and I0 (0|0).

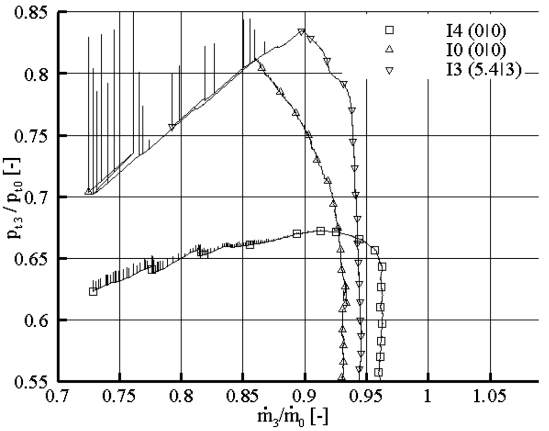

Fig. 9 Performance curves of the configurations I4 (0|0), I0 (0|0), I3 (5.4|3).

Fig. 10 Flow topology of the configuration I3 (5.4|3) in nominal operation range (SLR camera).

this configuration starts later. The schlieren photograph supports this explanation (Fig. 8). The bleed duct enables the flow to start leading to a characteristic shock system. The bleed gap forces a small amount of air flow to leave the intake through the bleed duct. The pressure recovery increases, as the low-energetic boundary layer of the ramp is removed by suction and the weaker shock boundary layer interaction leads to lower pressure losses.

To avoid a high mass flow rate loss, the bleed gap is decreased for the subsequent experiments. In the test configuration I3 (5.4|3) three insert elements were mounted to the bleed duct upstream wall to decrease the width of the bleed gap (Table 1). Also the diffuser was displaced by 5.4 mm in the horizontal direction and 3 mm in the vertical direction. Both the mass flow rate and the pressure recovery increase in respect to the configuration I0 (0|0). Compared to the first configuration I4 (0|0) without a bleed gap, the mass flow rate decreases, but the pressure recovery is greatly improved. For the configuration I3 (5.4|3), the maximum mass flow rate has a value of $\dot{m}_3/\dot{m}_0 = 0.95$ and the maximum pressure recovery is $p_{t,3}/p_{t,0} = 0.83$ (Fig. 9). The increase of mass flow rate, compared to the configuration I0 (0|0), is caused by the reduction to the bleed gap. The vertical and horizontal displacement of the diffuser results in a higher pressure recovery. The shearing off of the low-energetic boundary layer of the ramp leads to a weak interaction between the shocks and the boundary layer. The schlieren photograph (Fig. 10) clearly shows the differences of the flow stream pattern. In this configuration the first lip shock is removed by suction into the bleed gap and the second lip shock hits the edge of the isolator. The effect is that the boundary layer of the isolator is substantially thinner compared to Fig. 8.

Compared to the configuration I3 (5.4|3), in the case of the last configuration I4 (5.4|3) the size of the bleed gap is reduced from 10.8 mm to 5.4 mm by installing one more insert. The bleed gap of 5.4 mm is achieved by the horizontal downstream displacement of the diffuser. The vertical displacement of the diffuser remained at 3 mm. Figure 11 shows the effect of the configuration I4 (5.4|3) and the results of all four configurations for comparison. The last configuration did not affect the mass flow rate as expected. The mass flow rate is $\dot{m}_3/\dot{m}_0 = 0.95$, which is similar to the configuration I3 (5.4|3). Moreover, the pressure recovery of the configuration I4 (5.4|3) with $p_{t,3}/p_{t,0} = 0.81$ is less than the one for the configuration I3 (5.4|3). This behavior can be explained as follows: In the supercritical condition region of operation, where the two configurations have the same values for mass flow rate and pressure recovery (see Fig. 11, supercritical condition), the bleeding is not very efficient. When the large differences are considered between the bleed gap width of the configurations I4 (0|0) and I0 (0|0) (Table 1), it seems that the diffuser is more efficient with a vertical displacement (step-up) than a pure horizontal gap with respect to the suction of the boundary layer flow, that is, higher mass flow rate losses. Whereas the horizontal bleed gap allows a removal of only a part of the boundary layer flow, a step-up bleed gap allows the boundary layer flow almost to completely shear off. When the back pressure is increased by throttle position, the normal shock moves upstream to the bleed gap (critical condition) and the pressure in the bleed area of the intake increases. Because of the increasing pressure difference between the bleed gap entrance and bleed duct exit, more air from the boundary layer flow is removed by suction. Because compared to the configuration I4 (5.4|3) the width of the bleed gap of the configuration I3 (5.4|3) is larger, 10.8 mm instead of 5.4 mm, more low-energy boundary layer flow can be forced out when the normal shock is close to the critical cross section. This results in a weaker

Fig. 8 Flow topology of the configuration I0 (0|0) in nominal operation range (SLR camera).

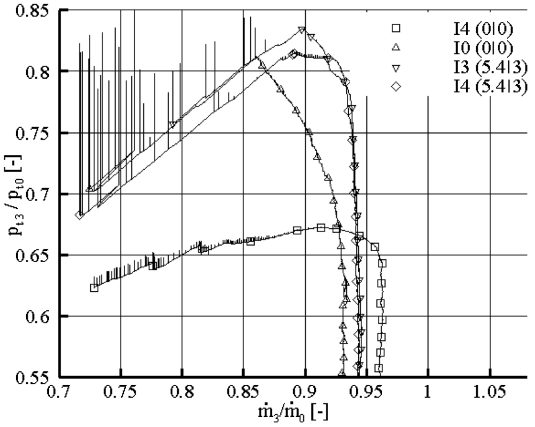

Fig. 11 Performance curves of the configurations I4 (0|0), I0 (0|0), I3 (5.4|3), and I4 (5.4|3).

shock boundary layer interaction, therefore a higher pressure recovery.

A. Supercritical Condition

The effects of the different configurations and geometries on the flow phenomena inside the intake are discussed. Schlieren photographs and video sequences, taken by the high-speed schlieren camera, are used to show these phenomena.

A Schlieren photograph of the intake flow of configuration I4 (0|0) is shown in Fig. 12. During the supercritical condition the mass flow rate remains constant, whereas the pressure recovery increases. In this situation, the normal shock moves from the end of the diffuser upstream to the critical throat section. The separation of the boundary layer on the ramp and its thickening, caused by the shocks that are generated at the cowl, avoids the start of the intake. High pressure losses due to the separated shock ahead of the cowl lead to the low pressure recovery of $p_{t,3}/p_{t,0} = 0.56$. The boundary layer flow expands at the concave interface between the ramp and the diffuser and interacts with the reflected shocks from the cowl. The expansion fan deflects the boundary layer being nearly parallel to the diffuser contour (Fig. 12). By suction, the low-energy boundary layer is removed through the bleed gap, and a shock system establishes in the intake configuration I0 (0|0). The boundary layer separates just at the beginning of the diffuser which indicates the geometry does not have the correct design. The unsteady connection of the isolator and diffuser is assumed to be the reason for the separation. Because of the separation of the boundary layer the effective duct height at the rear part of the diffuser is only half the size that is geometrically possible. Therefore, the subsonic flow decelerates less, and the pressure recovery increases less than the condition without boundary layer bleed gap. For approximately the same throttle position $A_4/A_0 = 0.67$ as for the configuration I4 (0|0), the pressure recovery reaches $p_{t,3}/p_{t,0} = 0.53$. Up to the pressure recovery of approximately $p_{t,3}/p_{t,0} = 0.64$ these two configurations have similar performances (Fig. 7). With boundary layer bleed gap, however, as in the case of configuration I0 (0|0), this value can be increased.

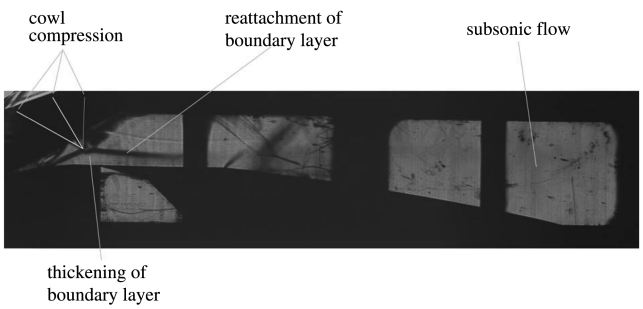

Fig. 12 Schlieren picture of the configuration I4 (0|0) at $A_4/A_0 = 0.66$ (high-speed camera).

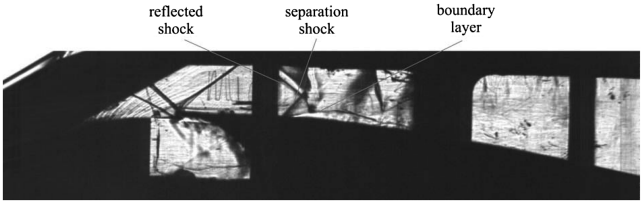

Fig. 13 Schlieren picture of the configuration I3 (5.4|3) at $A_4/A_0 = 0.56$ (high-speed camera).

The stated early separation can also be seen in the case of configuration I3 (5.4|3). But for this configuration, the effective diffuser duct height is larger than for configuration I0 (0|0). For that reason the pressure recovery is higher than for configuration I0 (0|0). The normal shock moves upstream during the changes to the throttle position as shown in Fig. 13. The separation that moves upstream along with the normal shock causes a separation shock. This separation shock crosses the shocks that are reflected by the cowl. In the supercritical condition there are no differences between the configurations I4 (5.4|3) and I3 (5.4|3) as shown in Fig. 11. The values for the pressure recovery and the mass flow rate of the two configurations are almost identical.

Another fact derived from the high-speed video sequences is that the flow inside the intake is unsteady even in the supercritical condition. This happens mainly in the region, where the flow separates on the diffuser. The separation does not remain at a constant point, but moves around the interface between the isolator and the diffuser. These rapid movements cause the unsteady behavior of the flow already during the supercritical condition. This condition leads to an unsteady pressure level at the entrance of the combustion chamber.

B. Bleeding

The bleeding system of an intake is designed to be effective when the normal shock is located in the direct vicinity of the bleed duct. In this situation, the pressure difference between the intake flow and the external flow is high enough to force part of the flow to flow through the bleed gap. The suction of the boundary layer leads to a decrease of the mass flow rate and an increase of the pressure recovery.

Figure 14, taken at the throttle position $A_4/A_0 = 0.51$, shows the flow condition for configuration I0 (0|0). The figure shows how the shock at the edge of the isolator interacts with the two shocks originating from the cowl. Because of this interaction, the shock originating from the isolator is deflected to the right. Further downstream, the shocks are reflected at the upper slip line. Also, two sharp shocks that decelerate the flow to subsonic velocity are visible a short distance further downstream . Up to this point, the suction is not yet fully effective, but by closing the throttle and thus increasing the back pressure, the boundary layer suction is intensified. Therefore, the mass flow rate decreases and the pressure recovery increases. How intensely the intake flow is affected is shown in Fig. 15. Here the

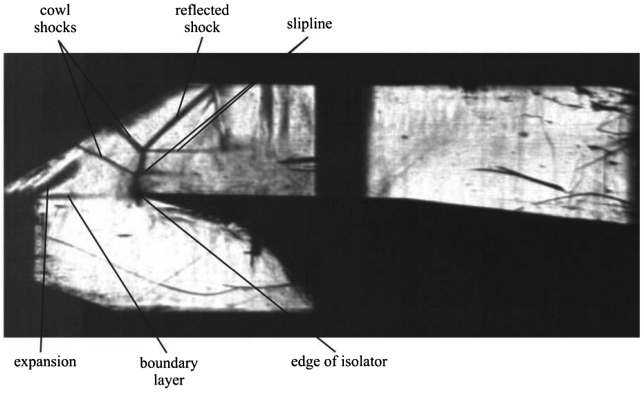

Fig. 14 Schlieren picture of the configuration I0 (0|0) at $A_4/A_0 = 0.51$ (high-speed camera).

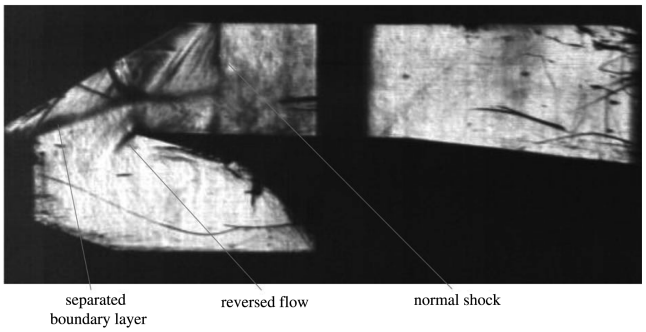

Fig. 15 Schlieren picture of the configuration I0 (0|0) at $A_4/A_0 = 0.41$ (high-speed camera).

higher isolator pressure causes the boundary layer of the ramp to separate. The dark schlieren pattern at the edge of the isolator is a result of the reverse flow in the boundary layer. On the isolator only a normal shock is seen and is located close to the critical throat section, that is, the condition with the maximum pressure recovery of $p_{t,3}/p_{t,0} = 0.80$ (Fig. 7).

In Fig. 16, the intake flow of configuration I3 (5.4|3) is shown at a throttle position of $A_4/A_0 = 0.51$, compared to the configuration I0 (0|0), where a different flow topology is observed. The lower cowl shock reaches into the bleed duct and, therefore, does not impact the flow over the isolator. The reason for that is the displacement of the diffuser in the x direction. Only the upper cowl shock creates a slip line when it interacts with the shock that originates from the edge of the isolator. This slip line proceeds very close and parallel to the surface of the isolator. Contrarily to configuration I0 (0|0), a short shock train, consisting of normal shocks, appears. The normal shocks are not reflected at the surface of the isolator, but at the separated boundary layer. In the bleed duct, it is visible that the air only flows in the downstream half of the duct. This can be seen at the two dark regions in the downstream half of the bleed duct. That indicates that the suction is not effective over the entire range of the bleed gap. Therefore, it is concluded that the shearing off of the flow due to the diffuser displacement in vertical direction is the main reason for the suction of boundary layer flow, that is, a reduction in the mass flow rate.

In Fig. 17, the flow is shown for the throttle position $A_4/A_0 = 0.41$, when the normal shock remains at the critical throat section so that the intake is in the critical condition. The maximum pressure recovery $p_{t,3}/p_{t,0} = 0.83$ is received in this condition. The position of the normal shock is influenced by the interaction of the ramp expansion and the cowl shock. Behind the normal shock, the flow can expand along the entire diffuser, while the pressure recovery reaches the maximum. Furthermore, the beginning of a slip line can be seen at the interception point. By shearing off the boundary layer of the ramp, the flow on the isolator is influenced less by the boundary layer that starts at the edge of the isolator.

The flow topology of a smaller bleed gap can be seen in the schlieren photographs. They show the intake flow of the configuration I4 (5.4|3) at the throttle position $A_4/A_0 = 0.51$. Only few differences are observed compared to the latter configuration.

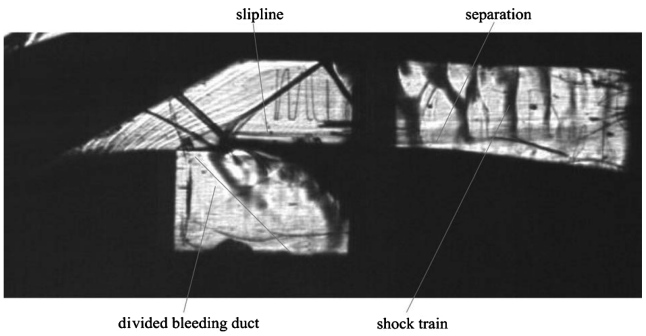

Fig. 16 Schlieren picture of the configuration I3 (5.4|3) at $A_4/A_0 = 0.51$ (high-speed camera).

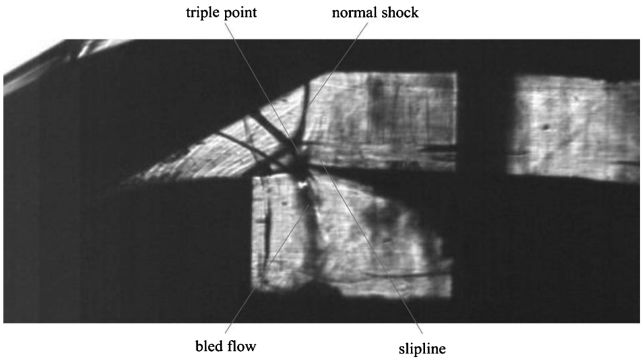

Fig. 17 Schlieren picture of the configuration I3 (5.4|3) at $A_4/A_0 = 0.41$ (high-speed camera).

For example, the bleed gap is not divided as noticeably as the one of the previous configurations, but the flow streams along the concave wall. The slip line that originates where the cowl shock and the shock of the edge of the isolator cross can be seen for this configuration, too. In the rear region of the shock train, it is remarkable that the shocks enter the slip line and are reflected at the boundary layer.

Because the differences of the flowfields are very small, the pressure recovery of configuration I4 (5.4|3) $p_{t,3}/p_{t,0} = 0.70$ differs only slightly from configuration I3 (5.4|3). However, when the back pressure is increased by using the throttle, the values for the configurations I3 (5.4|3) and I4 (5.4|3) start to differ substantially.

The conclusions of the previous observations are that the performance of an intake can be improved by displacing the diffuser in horizontal and vertical direction. In the condition of the diffuser displacement in vertical direction, the boundary layer flow of the ramp is sheared off. This stops the boundary layer to thicken due to the pressure increase and its separation. With a horizontal displacement, the shocks that originate from the cowl lip (Fig. 12) can be sucked into the bleed duct. Therefore the pressure losses due to the shock boundary layer interactions can be decreased. Overall, it can be said that the combination of the horizontal and vertical displacement provides the best performance for this intake. A comparison of the configurations I3 (5.4|3) and I4 (5.4|3) shows that a bleed gap size of 10.8 mm is more efficient than 5.4 mm to increase the maximum pressure recovery.

V. Unsteady Behavior of Different Configurations

The buzzing mode is investigated to determine the buzzing frequencies of the different configurations. One reason for buzzing is the Ferri-instability, of which slip lines are an indication [18]. A slip line is a discontinuity plane that separates two regions with different flow velocities and total pressures. The slip line is caused by the intersection of the shock originating at the ramps and the normal shock that moves upstream from the intake during the subcritical condition. The intersection point is called the triple point. The position of the triple point depends on the angle of the ramp shocks and the distance of the normal shock to the cowl lip. If a slip line enters the intake, the Ferri-instability can occur, causing the intake to buzz. Experiments show that planar intakes especially tend to be entered by a slip line and therefore cause the Ferri-instability. For each configuration, a certain throttle position which is gained by the performance chart is set and the buzzing is analyzed over a short time period. The fast Fourier transformation (FFT) analyses of the unsteady pressure measurements and the schlieren photographs taken with the high-speed camera are shown. Together, they give an impression of the unsteady behavior of the intake in this condition. The frequency of the buzzing is calculated by the FFT analysis and measured with the high-speed schlieren video sequences. The data acquisition rate for configuration I4 (0|0) was 1000 Hz. The data acquisition rate for configurations I0 (0|0), I3 (5.4|3), and I4 (5.4|3) was 500 Hz.

In Fig. 18, the results of the FFT analysis are shown. The measured pressure values of the two unsteady pressure sensors are shown as a

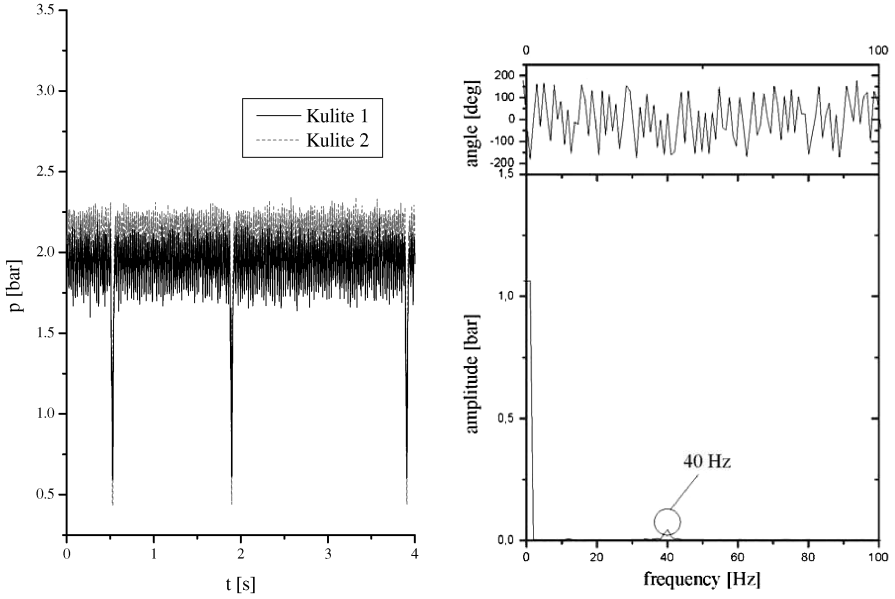

Fig. 18 Measured pressure for the configuration I4 (0|0); left: time history, right: FFT analysis.

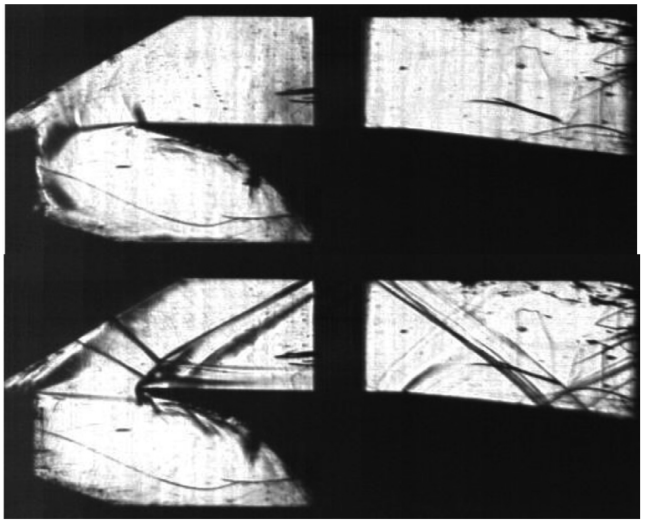

Fig. 19 Schlieren picture of the configuration I0 (0|0) while buzzing; top: unstarted, bottom: started (high-speed camera).

function of the time. By applying the FFT analysis to a certain time interval, the frequency spectrum is determined. To have sufficient values for the analysis, a time interval of $\Delta t = 1$ s is chosen. The analysis is completed by applying the Hanning window. As shown in Fig. 18, the FFT analysis for configuration I4 (0|0) gives a buzzing frequency of $f = 40.04$ Hz. This result agrees well with the result from the high-speed schlieren photographs that show a frequency of $f = 40$ Hz.

The effects of a bleed gap on the buzzing frequency is seen in the following pictures. For configuration I0 (0|0), Fig. 19 shows the flow condition for the unstarted (top) and started (down) intake. By an analysis of the high-speed schlieren pictures a buzzing frequency $f = 11.21$ Hz is measured. This frequency is substantially lower than the configuration I4 (0|0). The results of the FFT analysis of the unsteady pressure sensors are shown in Fig. 20. A slightly different buzzing frequency $f = 13.28$ Hz is given.

The last two configurations, I3 (5.4|3) and I4 (5.4|3), do not differ substantially from the configuration I0 (0|0). The presence or absence of a bleed gap has a strong influence on the buzzing frequency. To prove this, the high-speed schlieren pictures and FFT analyses for the configurations I3 (5.4|3) and I4 (5.4|3) are shown.

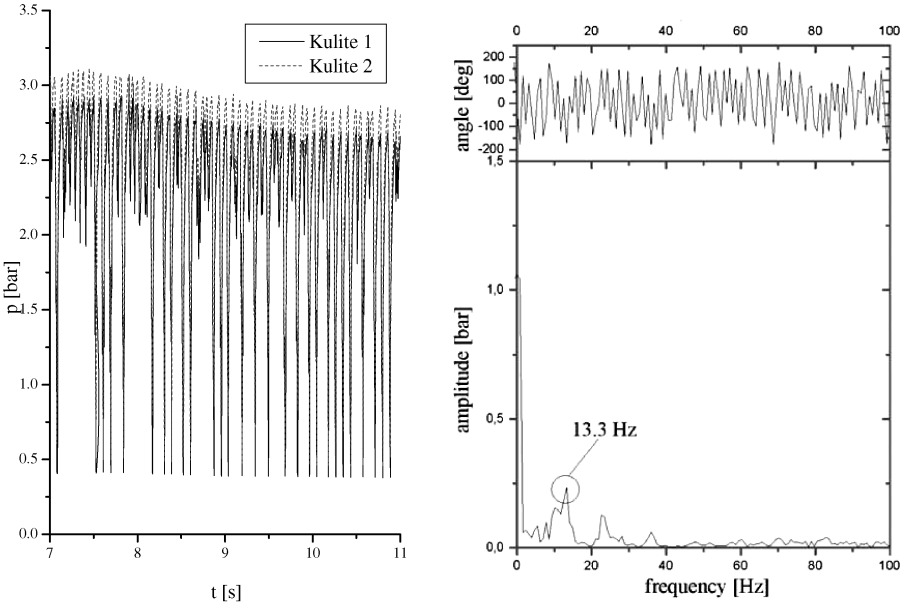

Fig. 20 Measured pressure for the configuration I0 (0|0); left: time history, right: FFT analysis.

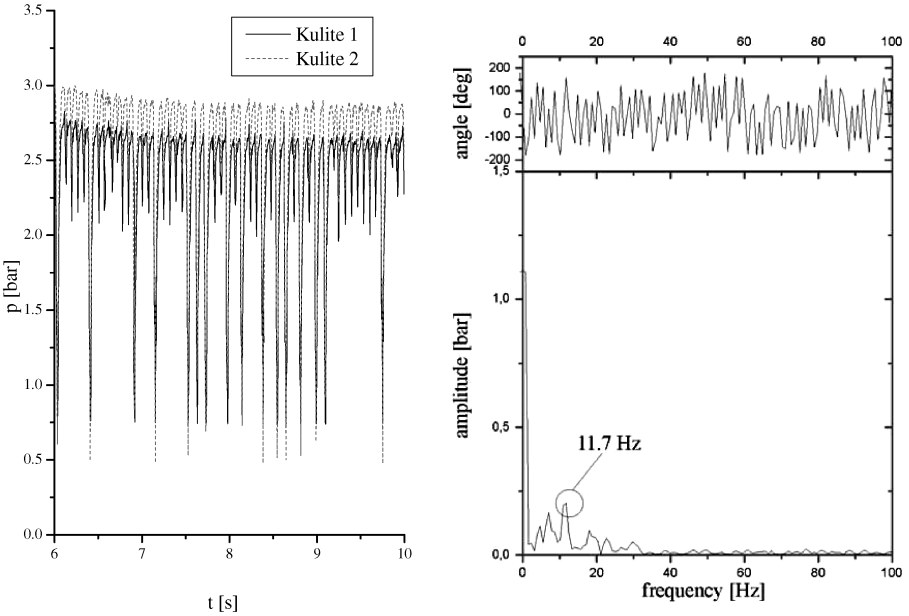

Fig. 21 Measured pressure for the configuration I3 (5.4|3); left: time history, right: FFT analysis.

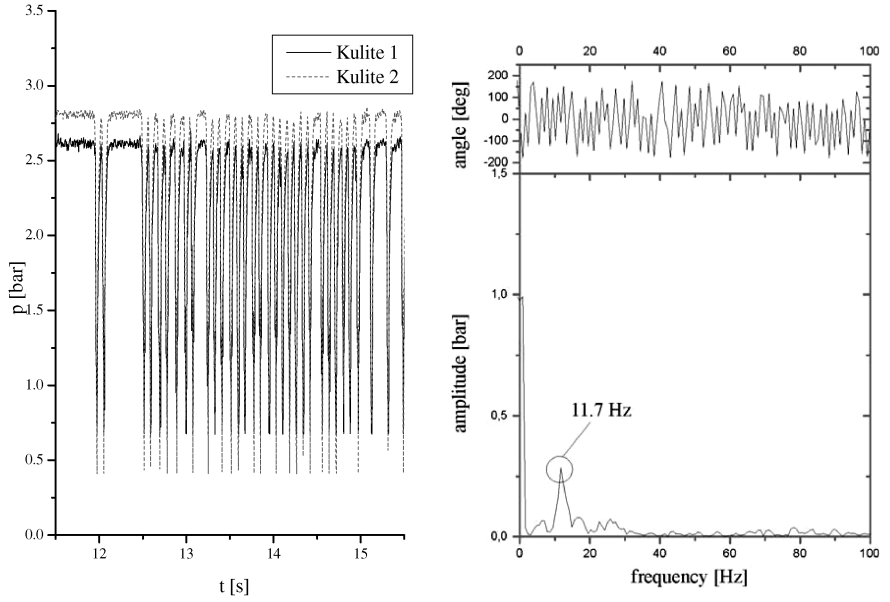

Fig. 22 Measured pressure for the configuration I4 (5.4|3); left: time history, right: FFT analysis.

From high-speed schlieren pictures the buzzing frequencies $f = 14.1$ Hz and $f = 12.3$ Hz are measured for the configurations I3 (5.4|3) and I4 (5.4|3), respectively. The FFT analysis gives the buzzing frequency $f = 11.72$ Hz for both configurations (Fig. 21 and 22). The differences between the values that are derived from schlieren photographs and those calculated by the FFT analysis result from the inaccurate determination of beginning and end of the buzzing in the schlieren video sequences.

VI. Conclusions

The flow properties for several intake configurations were investigated by the high-speed schlieren technique and by pressure measurements, to obtain the performance charts and the buzzing frequencies for each single intake configuration.

The influences of the shock boundary layer interactions and the boundary layer separation on the performance characteristics, that is, the mass flow rate and pressure recovery, are very dominant. The shock boundary layer interactions and the boundary layer separation depend on the geometry of the intake. The shape of the diffuser causes the boundary layer to separate at the interface between isolator and diffuser. Because the position of the boundary layer separation is unstable, unsteady flow phenomena occur and lead to unsteady flow properties at the entrance of the combustion chamber. The shearing off of the boundary layer flow by means of the vertical displacement of the diffuser is an efficient method to keep the shock boundary layer interaction and flow separation weak, which leads to a high pressure recovery. This measure combined with an optimum position and width of the bleed gap that avoids any reflection of the cowl shock improves the performance of the intake. The experiments proved that the existence of a bleed gap and the geometry of the diffuser highly influence the unsteady flow phenomena inside the intake. These unsteady flow properties were observed in the boundary layer separation regions at the interface between isolator and diffuser and during the buzzing state of the intake.

The buzzing frequency of an intake with a bleed gap is lower than of one without a bleed gap. The buzzing behavior also depends on the configuration geometry for each intake. Without bleeding in the condition of the configuration I4 (0|0) the buzzing frequency is approximately 40 Hz and with a bleed gap the buzzing frequency of

configuration I0 (0|0) decreases to 13.28 Hz. The vertical displacement of the diffuser in the condition of configurations I3 (5.4|3) and I4 (5.4|3) gives a decrease of the frequency to 11.72 Hz.

These results show that this intake needs to have a configuration with a bleed gap of a critical size and a vertical displacement of the diffuser to provide a high performance and a low buzzing frequency. This study also clearly shows that the presence of a bleed gap causes a delay of the buzzing phenomena.

References

[1] Curran, E. T., and Murthy, S. N. B., *Scramjet Propulsion*, AIAA Education Series, AIAA, Reston, VA, 2000.

[2] Rausch, V. L., Clinton, C. R., and Crawford, J. L., "Hyper-X: Flight Validation of Hypersonic Airbreathing Technology," ISABE Paper 97-7024, Sept. 1997.

[3] Sippel, M., and Koschel, W., "Parametrical Analysis of Near-Term Air-Breathing Engine Concepts for First Stage Space Plane Acceleration Missions," AIAA Paper 2000-3713, July 2000.

[4] Henckels, A., Kreins, A. F., and Maurer, F., "Experimental Investigations of Hypersonic Shock-Boundary Layer Interaction," *Journal of Flight Sciences and Space Research*, Vol 17, No. 2, 1993, pp. 116–124.

[5] Stockbridge, R. D., "Experimental Investigation of Shock Wave/Boundary-Layer Interaction in an Annular Duct," AIAA Paper 88-0272, 1988.

[6] Carrol, B. F., and Dutton, J. C., "Characteristics of Multiple Shock Wave/Turbulent Boundary Layer Interaction in Rectangular Ducts," AIAA Paper 88-3805, 1989.

[7] Seddon, J., and Goldsmith, E. L., *Intake Aerodynamics*, AIAA Education Series, AIAA, New York, 1985.

[8] Seddon, J., and Goldsmith, E. L., *Practical Intake Aerodynamic Design*, AIAA Education Series, AIAA, Washington, DC, 1993.

[9] Bissinger, N. C., "Inlet and Propulsion Integration of RAM Propelled Vehicles," *AGARD FDP Special Course on "Aerothermodynamics and Propulsion Integration for Hypersonic Vehicles"*, NATO, April 1996, pp. 8.1–8.45.

[10] Shih, T. I.-P., Rimlinger, M. J., and Chyu, W. J., "Three-Dimensional Show-Wave/Boundary-Layer Interactions with Bleed," *AIAA Journal*, Vol. 31, No. 10, Oct. 1993, pp. 1819–1826.

[11] Hahn, T. O., Shih, T. I.-P., and Chyu, W. J., "Numerical Study of Shock-Wave/Boundary Interactions with Bleed," *AIAA Journal*, Vol. 31, No. 5, May 1993, pp. 869–876.

[12] Harloff, G. J., and Smith, G. E., "Supersonic-Inlet Boundary-Layer Bleed Flow," *AIAA Journal*, Vol. 34, No. 4, April 1996, pp. 778–785.

[13] Heiser, W. H., and Pratt, D. T., *Hypersonic Airbreathing Propulsion*, AIAA Education Series, AIAA, Washington, DC, 1994.

[14] Wuest, W., *Strömungsmeßtechnik*, Friedr. Vieweg & Sohn, Braunschweig, Germany, 1969.

[15] Oertel, H., Sr., and Oertel, H., Jr., *Optische Strömungsmeßtechnik*, G. Braun, Karlsruhe, Germany, 1989.

[16] Settles, G. S., *Schlieren and Shadowgraph Techniques*, Springer–Verlag, New York, 2001.

[17] Esch, H., "Die 0.6 m × 0.6 m—Trisonische Meßstrecke (TMK) der DFVLR in Köln-Porz (Stand 1986)," DFVLR-Mitt. Report 86-21, Köln, Germany, 1986.

[18] Krohn, E.-O., and Triesch, K., "Untersuchungen zur Ferri-Instabilität bei Überschalleinläufen," DFVLR-Forschungsbericht Report 85-53, Köln, Germany, 1985.

[19] Koschel, W., Niehuis, R., and Reinmöller, U., "Luftfahrtantriebe II," *Vorlesungsskript*, RWTH-Aachen, Aachen, Germany, 2000.

T. Shih
Associate Editor